Available online at www.sciencedirect.com
SCIENCE DIRECT®
Remote Sensing of Environment 85 (2003) 282–289
Remote Sensing of Environment
www.elsevier.com/locate/rse

Satellite-measured growth of the urban heat island of Houston, Texas

David R. Streutker*

Department of Physics and Astronomy, Rice University, Houston, TX 77005, USA

Received 14 June 2002; received in revised form 9 December 2002; accepted 11 December 2002

Abstract

Growth of the surface temperature urban heat island (UHI) of Houston, TX is determined by comparing two sets of heat island measurements taken 12 years apart. Individual heat island characteristics are calculated from radiative temperature maps obtained using the split-window infrared channels of the Advanced Very High Resolution Radiometer (AVHRR) on board National Oceanic and Atmospheric Administration polar-orbiting satellites. Eighty-two nighttime scenes taken between 1985 and 1987 are compared to 125 nighttime scenes taken between 1999 and 2001. Analysis of the UHI characteristics from these two intervals reveals a mean growth in magnitude of 0.8 K, or 35%. The growth of the mean area of the UHI is found to range between 170 and 650 km^2, or from 38% to 88%, depending on the method of analysis.
© 2003 Elsevier Science Inc. All rights reserved.

Keywords: Urban heat island; Radiative temperature map; Remote sensing

1. Introduction

One of the most well known forms of anthropogenic climate modification is the phenomenon of urban heating. Modification of land-cover in urban areas can cause the local air and surface temperatures to rise several degrees higher than the simultaneous temperatures of the surrounding rural areas. This effect is often referred to as the urban heat island (UHI) and has been documented for over 150 years (Howard, 1833). Over the past few years, UHI's have been studied in cities as diverse as Lódź, Poland (Klysik & Fortuniak, 1999), Reykjavík, Iceland (Steinecke, 1999), Fairbanks, AK (Magee, Curtis, & Wendler, 1999), and Granada, Spain (Montávez, Rodríguez, & Jiménez, 2000).

Urban heat island studies are generally conducted in one of two ways: measuring the UHI in air temperature through the use of automobile transects and weather station networks, and measuring the UHI in surface (or skin) temperature through the use of airborne or satellite remote sensing. In situ data have the advantage of a high temporal resolution and a long data record, but have poor spatial resolution. Conversely, remotely sensed data has higher spatial distribution but low temporal resolution and a shorter data record. Highly accurate remotely sensed temperature measurement also requires the use of concurrent ground truth data and/or radiosonde data in order to correct for infrared absorption and reradiation by various atmospheric components, most notably water vapor (François & Ottlé, 1996).

In recent years, the field of remote sensing has lent itself well to the study of UHI's. Roth, Oke, and Emery (1989) and Gallo and Tarpley (1996) used remote sensing techniques to compare the UHI effect to vegetation index. Owen, Carlson, and Gillies (1998) used fractional vegetation cover and surface moisture availability to study the impact of urbanization in and around State College, PA. While the above studies used Advanced Very High Resolution Radiometer (AVHRR) data, Kawashima, Ishida, Minomura, and Miwa (2000) used Landsat 5 data to study the relationship between surface temperature and air temperature during winter nights in Japan and found that the effect of the surface temperature on air temperature was related to the mean lapse rate of the atmospheric boundary layer.

To date, the vast majority of climatological studies of UHI's have been performed using in situ data, due in large part to the brevity of the remotely sensed data record. Karl, Diaz, and Kukla (1988) found that throughout the last century, urbanization has created a warm bias of 0.06 K in the climate record of the United States. Wang, Zeng, and Karl (1990) found an increase of 0.1 K per decade in the UHI's throughout China since the late 1970s. The purpose

* Tel.: +1-713-348-3644; fax: +1-713-348-5143.
E-mail address: streutke@rice.edu (D.R. Streutker).

0034-4257/03/$ - see front matter © 2003 Elsevier Science Inc. All rights reserved.
doi:10.1016/S0034-4257(03)00007-5

of this study is to use remote sensing techniques to measure the change in the surface temperature UHI of Houston, TX over the course of a 12-year period, from 1987 to 1999.

2. Area of study

The subject of this study is Houston, TX, a city of 1.95 million people (U.S. Bureau of Census, 2001). Houston has undergone a period of significant growth in the last decade, including a 20% increase in inhabitants from the 1990 population of 1.63 million (U.S. Bureau of Census, 1996). Geographically, Houston is well suited to an analysis by remote sensing means. A lack of city zoning laws has led to large amounts of urban sprawl, resulting in a city of large area and relatively low population density. The city of Houston has an area of approximately 1400 km^2 and is located at 95.4°W and 30.0°N on the upper Texas Gulf Coast, an area lacking significant orographic features.

3. Method and data sources

Urban heat island measurements are determined from surface temperature maps of the Houston, TX region derived from radiation data obtained by the AVHRR satellite instrument on board the NOAA-9 and NOAA-14 satellites. Data are obtained for numerous scenes over two discrete time intervals. Eighty-two relatively cloud-free images are obtained for the 2-year interval of March 1985 through February 1987 (interval 1) by the NOAA-9 instrument. One hundred and twenty-five relatively cloud-free images are obtained for the 2-year interval of July 1999 through June 2001 (interval 2) by the NOAA-14 instrument. The monthly distribution of the images within the two intervals is shown in Fig. 1. Each of the images was taken during the descending pass of the satellite, between the hours of 0200 and 0530 LST (0800–1130 GMT). Only images with satellite zenith angles less than 20° are used, as images with high zenith angles may be subject to larger uncertainties due to the lengthened atmospheric path (Prata, 1993).

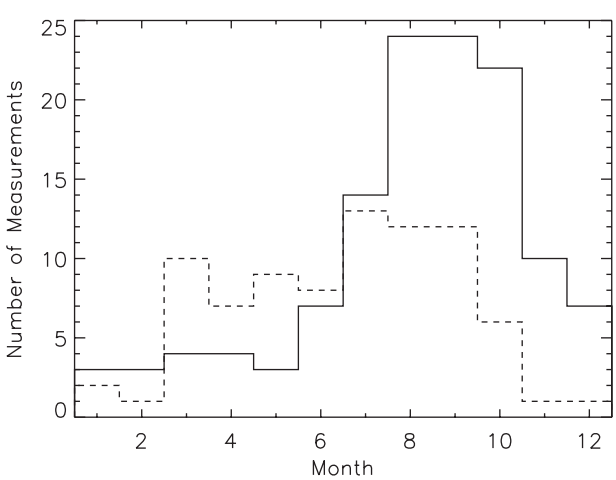

Fig. 1. The monthly distribution of the UHI measurements. The dashed line shows the number of measurements within interval 1, and the solid line shows the number of measurements within interval 2.

Radiance values are calculated for the "split-window" channels 4 (10.3–11.3 μm) and 5 (11.5–12.5 μm) using the calibration coefficients contained within the ephemeris data. These radiance values are then corrected for the non-linearity of AVHRR channels 4 and 5 using radiance correction coefficients (Kidwell, 1998). The corrected radiance values (R_i) are then converted to brightness temperatures by using the inverse of Planck's equation of radiation:

$$T_i(R_i) = \frac{C_2 v_j}{\ln\left(1 + \frac{C_1 v_j^3}{R_i}\right)} \tag{1}$$

The constants in Eq. (1) are $C_1 = 1.1910659 \times 10^{-5}$ mW m^{-2} sr^{-1} cm^4 and $C_2 = 1.438833$ cm K, with v_j the central wave number of each channel. The brightness temperature data from the split-window channels is then used to calculate the surface temperature using the technique of Price (1984):

$$T_{\text{surface}} = T_4 + R(T_4 - T_5) \tag{2}$$

where T_4 and T_5 are the brightness temperatures of channels 4 and 5 and $R = 1/[(\beta_5/\beta_4 - 1)] = 3.33$ (β_4 and β_5 are atmospheric absorption coefficients for channels 4 and 5).

Surface temperature maps of each scene are used to make individual UHI measurements using a method similar to the one described by Streutker (2002). This technique uses a least-squares fit of the entire heat island to a Gaussian surface of the form

$$T(x,y) = T_o + a_1 x + a_2 y + a_o \times \exp\left[-\frac{((x-x_o)\cos\phi + (y-y_o)\sin\phi)^2}{0.5a_x^2} - \frac{((y-y_o)\cos\phi - (x-x_o)\sin\phi)^2}{0.5a_y^2}\right] \tag{3}$$

This method provides not only a measure of the UHI magnitude representative of the entire city (a_o), but also of the spatial extent (a_x and a_y), orientation (ϕ), and central location (x_o and y_o) of the heat island as well. This method is also used to determine the spatial gradients (a_1 and a_2) and mean value (T_o) of the surface temperature of the surrounding rural area. Fig. 2 shows an example of such a Gaussian surface.

In order to perform the fit, a land temperature image is created by masking out all areas of clouds and open water. The region of the land temperature image that contains the urban area is then temporarily masked out, producing an image consisting entirely of rural pixels. As the exact spatial extent of the UHI is unknown prior to measurement, the urban mask must be large enough that it completely covers the urban pixels. It is inevitable then that some rural pixels

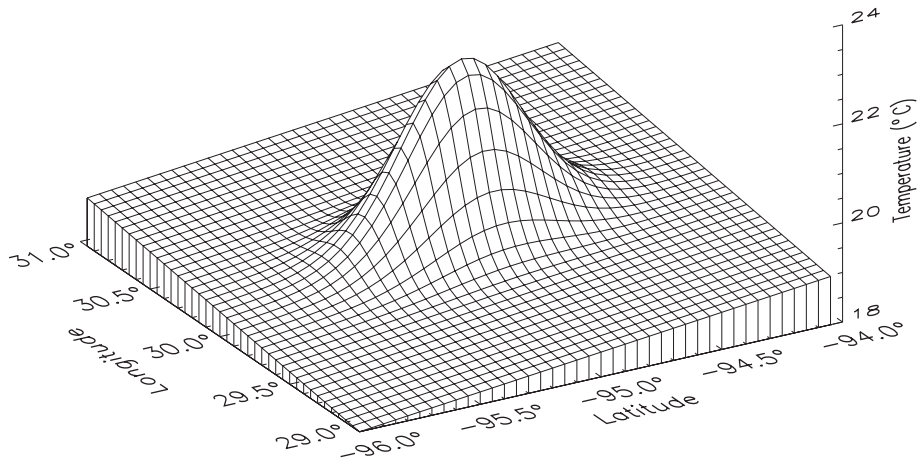

Fig. 2. An example of the Gaussian surface defined in Eq. (3). In this example, $T_o = 20$ °C, $a_1 = a_2 \simeq 5$ mK km^{-1}, $a_o = 3.5$ K, $a_x \simeq 60$ km, and $a_y \simeq 35$ km.

near the urban area are masked out as well. The urban mask does not change from image to image, resulting in all cloud-free rural images having the same number of rural pixels.

This rural temperature image is fit to a planar surface, resulting in the determination of T_o, a_1, and a_2. The rural temperature components (the first three terms on the right-hand side of Eq. (3)) are then subtracted from the land temperature image, leaving only the heat island signature. The temperature image of the UHI is then fit to a pure Gaussian surface (the exponential term on the right-hand side of Eq. (3)), which determines the UHI measurements. The UHI magnitude is the height of the Gaussian (a_o), and the longitudinal and latitudinal extents of the UHI are the Gaussian width parameters (a_x and a_y). The orientation (ϕ) and central location (x_o and y_o) of the UHI are also calculated in this step.

4. Discussion of error

Price (1984) cites three sources of error in the measurement of land surface temperature: radiometric calibration errors of less than 1 K, dependence of R on atmospheric absorption which can result in changes of temperature retrievals of order 2 K, and variations in surface emissivity which can result in changes in retrieved temperatures of order 1 K. These factors combine to produce an rms error of 2–3 K.

The split-window method of land surface temperature derivation can also be affected by emissivity differences between channels 4 and 5 as well as emissivities not equal to one. Becker (1987) uses radiative transfer theory to derive an error due to differences in emissivity of order

$$\Delta T \approx \frac{1-\bar{\varepsilon}}{\bar{\varepsilon}} \times 50\ \mathrm{K} - \frac{\varepsilon_4 - \varepsilon_5}{\bar{\varepsilon}} \times 300\ \mathrm{K} \tag{4}$$

where ε_4 and ε_5 are the surface emissivities in channels 4 and 5, and $\bar{\varepsilon}$ is the average of the two. One should note that the error due to differences in emissivity is six times greater than the error due to nonunity emissivities, and that if ε_4 is greater than ε_5, the errors will partially cancel. In their UHI analysis, Henry, Dicks, Wetterqvist, and Roguski (1989) assume emissivity values of $\varepsilon_4 = \varepsilon_5 = 0.97$, which result in a temperature bias of +1.5 K. Vidal (1991) finds $\varepsilon_4 - \varepsilon_5 = -0.011$ for agricultural surfaces, resulting in a temperature bias of −3.1 K. Unfortunately, there is little available information concerning the comparable emissivities of urban surfaces.

A major advantage of studying the UHI is that the quantity of interest is not the absolute urban temperature, but the difference in temperature between the urban and rural areas. The sources of error listed above are systematic and are thus partially removed in the differencing procedure. However, a significant source of error in this study may in fact be due to spatial differences in emissivity between the urban area and the surrounding rural area. Urban surfaces tend to have slightly lower emissivities than rural, vegetative ones (Oke, 1978; Rees, 1990). A difference in emissivity of at least 0.01 is quite likely and would thus cause the UHI magnitudes to be underestimated by a degree or more. Due to the uncertain nature of the errors described above, no attempt is made to correct for them in this study.

5. Results

5.1. UHI magnitude

For interval 1, the mean rural temperature of the area surrounding the city of Houston is 17.2 ± 0.7 °C (the uncertainty quoted is the standard deviation of the mean and does not include any attempt to quantify the errors discussed in the previous section). The mean rural temperature of the same area for interval 2 is 17.1 ± 0.8 °C, virtually identical to the earlier interval. Temperature histograms of both of these sets of data are shown in Fig. 3. Due to the differing number of measurements in the two intervals, each histogram is normalized according to the number of measurements in the corresponding interval. As can be

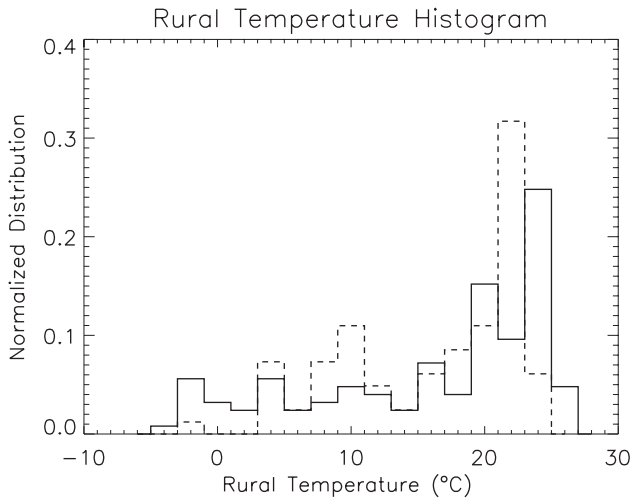

Fig. 3. A normalized histogram of rural temperatures. The dashed line shows the rural temperatures from interval 1, while the solid line shows the rural temperatures from interval 2. The two histograms show a great deal of similarity, indicating a lack of change in rural temperature between the two intervals.

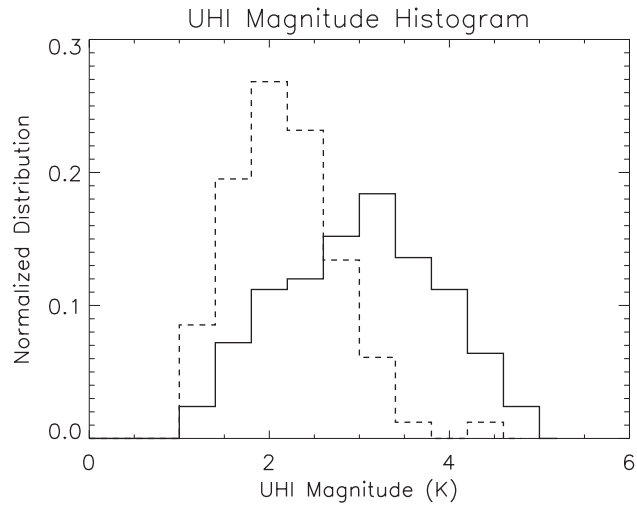

Fig. 4. A normalized histogram of the UHI magnitudes. The dashed line shows the UHI magnitudes from interval 1, while the solid line shows the UHI magnitudes from interval 2. The increase in UHI magnitude between the two datasets is apparent.

seen in this figure, a large fraction of the rural temperatures from both intervals lie in the range of 20–25°C, with the rest of the measurements spread evenly between 0 and 20°C. This distribution is due to the measurements being taken throughout the year and during a variety of temperatures. As can be seen in Fig. 1, the majority of the measurements was taken during the summer and early fall months, resulting in the high-temperature peak in Fig. 3. The fact that the mean rural temperature and its uncertainty for these two periods are so similar seems to indicate that there were no significant climatic differences in the region between the two intervals, and that the individual AVHRR instruments were well calibrated with respect to each other.

The mean UHI magnitude (a_o from Eq. (3)) for the 82 images in interval 1 is found to be 2.37 ± 0.07 K. The mean UHI magnitude for the 125 images in interval 2 is 3.19 ± 0.08 K, an increase of 0.82 ± 0.10 K. Fig. 4 shows histograms of the UHI magnitudes of both of these periods, normalized as in Fig. 3. The interval 1 data, shown with the dashed line, peaks at a lower temperature than the interval 2 data, which is shown with the solid line. The standard deviation of the set of interval 1 measurements is 0.60 K, while the standard deviation of the interval 2 set of measurements is slightly higher, at 0.86 K. These values are well within the uncertainty in measurement discussed in Section 4.

5.1.1. Seasonal considerations

As can be seen in Fig. 1, the UHI measurements are not distributed evenly throughout the year in either of the two intervals, most likely due to increased cloud cover during the cooler months. This led to concern that monthly differences in the UHI measurements could influence the statistical analysis. A bias could be introduced because a larger fraction of the interval 2 images were taken during the summer months than were the images in interval 1. In order to determine whether such a bias exists, a seasonal analysis was conducted.

Table 1 shows the mean UHI magnitude for each season. In each of the seasons, the mean UHI magnitude is greater for interval 2 than interval 1. The interval 1 seasonal mean (the mean of the four individual season means) is 2.35 ± 0.10 K, while the interval 2 seasonal mean is 3.10 ± 0.13 K. The difference between these two seasonal means is 0.75 ± 0.16 K, in very good agreement with the 0.82 ± 0.10 K difference found in the more general analysis conducted above.

5.1.2. Diurnal considerations

Due to differences in the orbit of the two satellites, the interval 2 data was taken an average of 90 min later in local time than the interval 1 data, as can be seen in Fig. 5. The interval 1 data points, shown as diamonds, were collected between 0230 and 0400 LST. The interval 2 data points, shown as asterisks, were collected between 0330 and 0530 LST. This led to concern that the difference in mean UHI magnitude was due, at least in part, to diurnal temperature variations and possibly the onset of solar insolation in the interval 2 data. Fig. 6 shows a plot of the average diurnal

Table 1
The mean UHI magnitudes for each season

	Interval 1 (K)	Interval 2 (K)
January–March	2.77 ± 0.21 (13)	3.45 ± 0.28 (10)
April–June	2.19 ± 0.10 (24)	2.51 ± 0.23 (14)
July–September	2.42 ± 0.09 (37)	3.36 ± 0.10 (62)
October–December	2.01 ± 0.18 (8)	3.11 ± 0.13 (39)
Seasonal mean	2.35 ± 0.10	3.10 ± 0.13

The numbers in parentheses are the total number of measurements in each season.

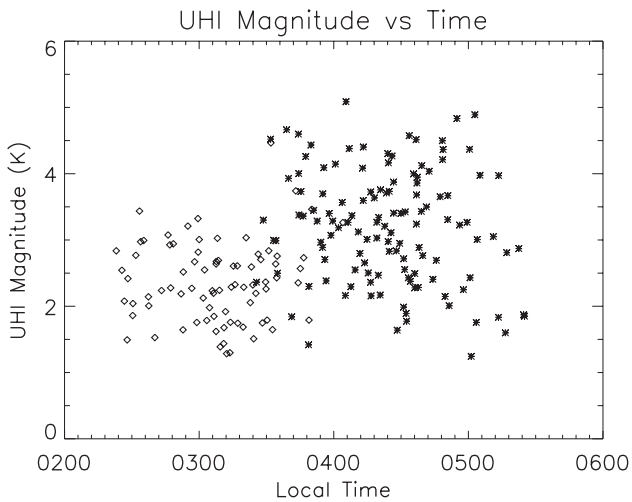

Fig. 5. A plot of UHI magnitudes versus local time. The diamonds represent the individual UHI magnitudes from interval 1, while the asterisks represent the individual UHI magnitudes from interval 2.

variations in air temperature during the year 2000 at the William P. Hobby International Airport, located in the southeastern part of the city of Houston (solid line). Also plotted are the average diurnal air temperatures for the months of January (dashed line) and July (dotted line). As can be seen from the graph, diurnal heating does not begin until at least 0500 LST, or after nearly all of the data was collected. A comparison of image collection times with sunrise times indicates that one or two of the images in interval 2 may have been taken as the sun rose.

If the UHI magnitudes are influenced by diurnal temperature variations (i.e. if the falling temperature during the night causes the UHI magnitudes to increase), then the magnitudes would be expected to show a correlation to the surface temperature, either rural or urban. This, however, does not seem to be the case. In fact, neither the interval 1 data nor the interval 2 data show any significant correlation with either rural temperature or local time. When correlated against rural temperature, the interval 1 data show a correlation coefficient of -0.1, while the interval 2 data show a correlation of -0.2 (this conflicts with the results of Streutker (2002), which may not have had a large enough sample size). It is thus unlikely that any of the data were affected by diurnal variations.

5.2. UHI spatial extent

The mean spatial extents (a_x and a_y from Eq. (3)) for the interval 1 UHI data are found to be 33.0 ± 1.3 km in longitude and 17.3 ± 0.5 km in latitude. The mean spatial extents for the interval 2 UHI data are found to be 40.5 ± 0.9 km in longitude and 19.6 ± 0.3 km in latitude. These values represent increases in extent of 23% in longitude and 13% in latitude. Fig. 7 shows a scatter plot of spatial extents of the heat islands. The interval 2 data, shown as asterisks, are on average above and to the right of the interval 1 data, which are shown as diamonds. This is due to the increased spatial extents of the interval 2 heat island signatures.

The two spatial extent parameters for each UHI measurement can be combined to determine the overall area or footprint of the UHI. The footprint itself has the form of an ellipse with the major and minor axes equivalent to the latitudinal and longitudinal extent parameters (this could be demonstrated by taking a horizontal cross-section through

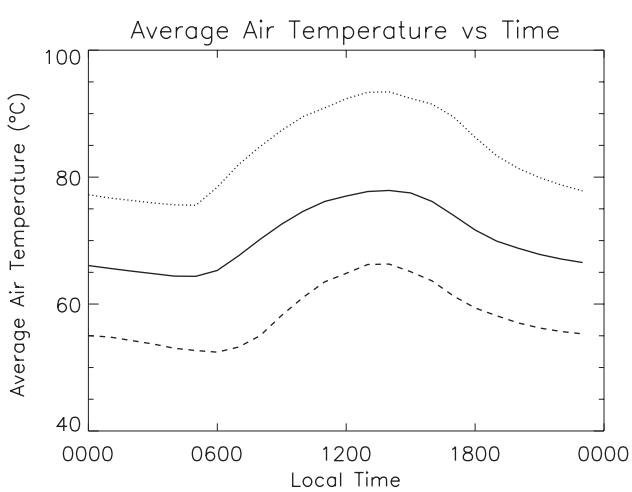

Fig. 6. A plot of the average local air temperature versus local time for the year 2000, as calculated from daily measurements. The solid line represents the average temperature throughout the entire year. The dashed and dotted lines represent the average temperatures throughout the months of January and July, respectively. The temperatures were measured at the William P. Hobby International Airport in Houston.

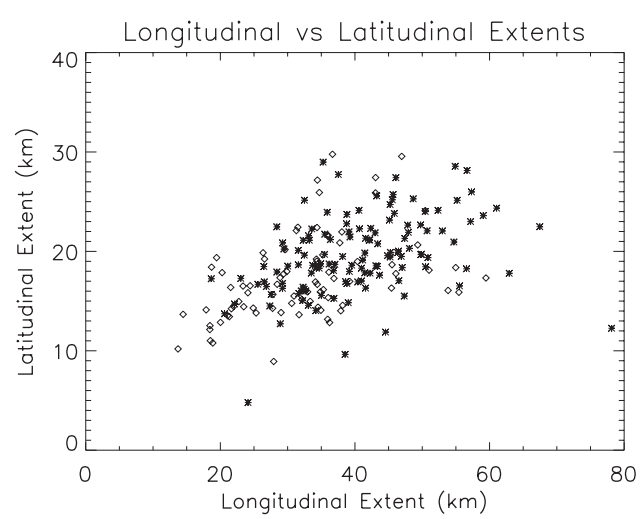

Fig. 7. A plot of UHI latitudinal and longitudinal extents. These spatial extents are determined using the Gaussian parameters a_x and a_y from Eq. (3). The diamonds represent the spatial extents from interval 1, while the asterisks represent the spatial extents from interval 2.

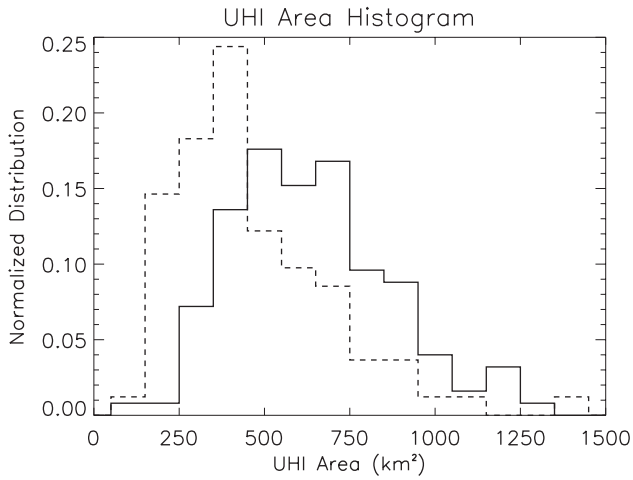

Fig. 8. A normalized histogram showing the area of the UHI's. The dashed line represents the interval 1 data, and the solid line shows the interval 2 data. The interval 2 UHI's have, in general, larger areas than the interval 1 UHI's.

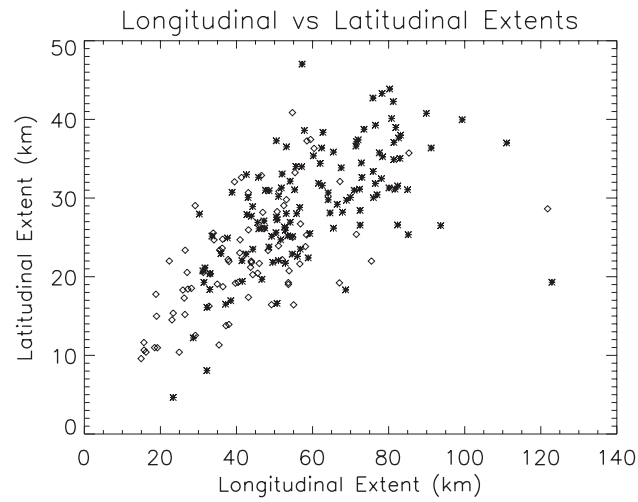

Fig. 10. A plot of UHI latitudinal and longitudinal extents. These spatial extents are determined using 1 K threshold method. The diamonds represent the spatial extents from interval 1, while the asterisks represent the spatial extents from interval 2 (note that the axes are different than those of Fig. 7).

the surface in Fig. 2). The area of each UHI can then be calculated as

$$\text{Area} = \frac{\pi a_x a_y}{4} \tag{5}$$

Using Eq. (5), the mean area for the interval 1 UHI data is found to be 450 ± 20 km^2. The mean area for the interval 2 UHI data is found to be 620 ± 20 km^2, an increase of 38%. A normalized histogram of individual area measurements is shown in Fig. 8, with the interval 1 data shown as the dashed line and the interval 2 data shown as the solid line.

By solving Eq. (3) for $x = a_x$ and $y = a_y$, one finds that the temperature is given by $T(a_x, a_y) = T_o + a_o e^{-1/2}$. Thus the spatial extents are defined as the distance from the center of the heat island at which the temperature falls to a level of $e^{-1/2}$, or 61%, of its maximum value. It may be that the spatial extents could be better understood if they represent the area of the UHI for which the temperature is greater than some absolute value instead of a fraction of the maximum value. By using a constant threshold, in this case of 1.0 K, the spatial extent is no longer dependent on the heat island magnitude and may better represent the entire footprint of the

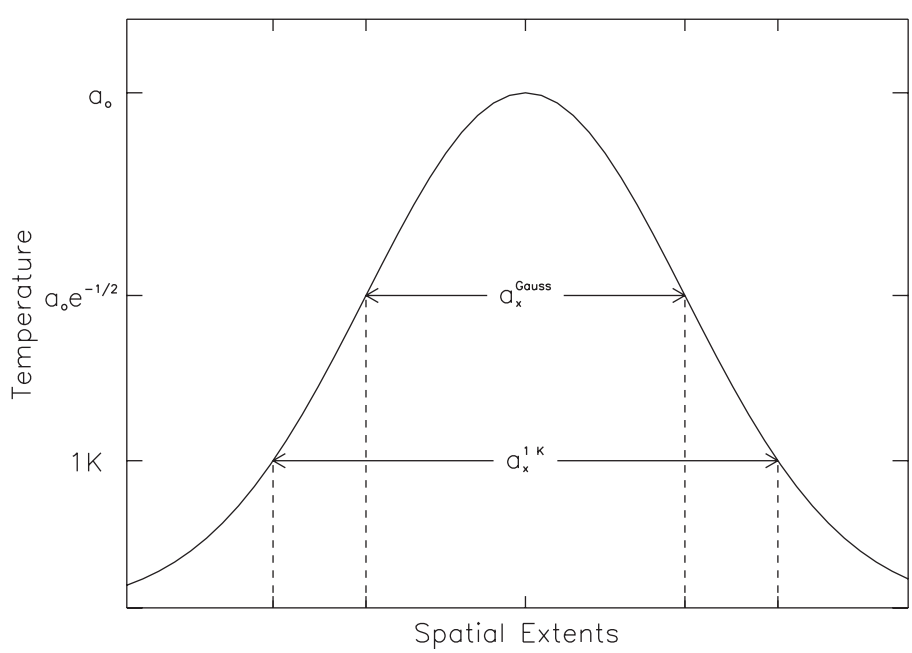

Fig. 9. A diagram showing the spatial extents based on the Gaussian and 1 K threshold methods of determination.

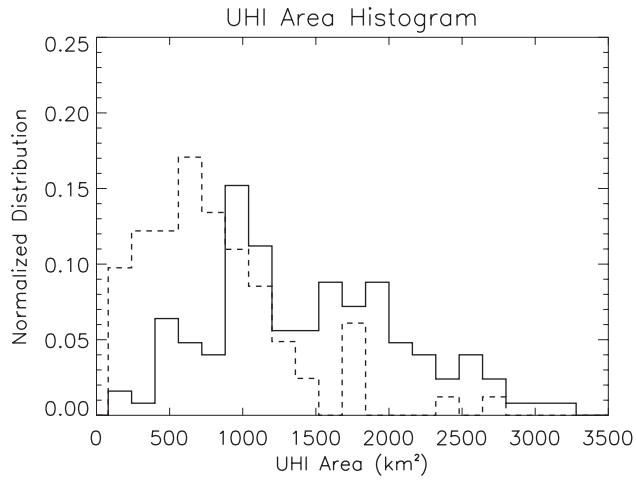

Fig. 11. A normalized histogram showing the area of the UHI's, using the 1 K threshold method of determining the spatial extent. The dashed line represents the interval 1 data, and the solid line shows the interval 2 data. The interval 2 UHI's have, in general, larger areas than the interval 1 UHI's.

heat island. The relationship between the 1 K spatial extents ($a_{x,y}^{1\ \mathrm{K}}$) and the previous Gaussian extents ($a_{x,y}^{\mathrm{Gauss}}$) is

$$a_{x,y}^{1\ \mathrm{K}} = a_{x,y}^{\mathrm{Gauss}} \times \sqrt{\frac{\ln a_o}{2}} \tag{6}$$

Fig. 9 further illustrates the relationship between a_x^{Gauss} and $a_x^{1\ \mathrm{K}}$.

When this method is used, the mean spatial extents for the interval 1 UHI data are found to be 42.4 ± 1.9 km in longitude and 22.2 ± 0.8 km in latitude, resulting in an area of 740 ± 40 km^2. The mean spatial extents for the interval 2 UHI data are found to be 60.4 ± 1.6 km in longitude and 29.2 ± 0.7 km in latitude for an area of 1390 ± 50 km^2. The increases in extent are 42% in longitude and 32% in latitude, resulting in a change in overall area of 88%. Fig. 10 shows a scatter plot of the spatial extents when the 1 K threshold is used. As with the Gaussian-based measurements, the interval 2 data are above and to the right of the interval 1 data. A normalized histogram of UHI areas calculated from the spatial extents is shown in Fig. 11, with the interval 1 data shown using the dashed line and the interval 2 data with the solid line.

6. Concluding remarks

Between 1990 and 2000, the city of Houston, TX grew in population by over 300,000 residents, an increase of nearly 20%. The Houston metropolitan area grew from 3.3 to 4.2 million persons, an addition of nearly 1 million residents. One manifestation of this considerable growth is a change in the heat island signature of the city.

Over the course of 12 years, between 1987 and 1999, the mean nighttime surface temperature heat island of Houston increased 0.82 ± 0.10 K in magnitude. It increased in area 170 ± 30 km^2 using the Gaussian method of area determination, and 650 ± 60 km^2 using the 1 K threshold method. It is curious to note that the growth of UHI, both in magnitude and spatial extent (using the Gaussian method of determination), scales roughly with the increase in population (extrapolated to 1987 levels), at approximately 30%. Also of interest is the large amount of variation shown in the UHI measurements, particularly in the UHI spatial extents. The UHI magnitudes varied over several degrees K, while the spatial extents varied over nearly an order of magnitude in area. It is well known that UHI magnitude depends on environmental variables such as wind speed, cloud cover, and atmospheric aerosol and water vapor content. The UHI spatial extent likely also depends on many spatial variables, such as surface moisture and vegetation cover, in addition to those listed above. This seems to be an indication that the UHI should be viewed as a dynamic meteorological phenomenon and not as a constant, uniform feature.

One unexpected possibility concerns the dependence of the UHI on urban population density as well as total population. It may be that while the spatial extent of the UHI is related to total urban population, the magnitude of the UHI may be more closely related to urban population density than overall population. Between 1990 and 2000, the population density of the city of Houston increased from 1200 km^{-2} to 1300 km^{-2}.

The natural progression of this work involves a continued monitoring of Houston's urban heat island to better quantify the relationship between population increase and heat island growth. As the record of remotely sensed data is extended, satellite-based climate studies will become more feasible. The record also continues to expand to include data from a growing number of platforms with high-resolution instruments. While low-resolution satellite data are adequate for studying the large-scale UHI characteristics, it may be beneficial to use high-resolution thermal data to compare heat island intensity to population density or land-cover on a smaller scale, such as that of individual neighborhoods. A relationship between population density and heat island intensity may be of interest to urban planners, who could monitor population density in an attempt to control or mitigate the affects of the UHI.

Acknowledgements

This work was supported by NASA's Office of Earth Science under Cooperative Agreement NCC-5-311 and by the Charles R. Conly Research Fund of Rice University. The author wishes to thank Dr. Patricia Reiff, Dr. Arthur Few, and Dr. Gary Morris, as well as three anonymous reviewers for their helpful comments and thoughtful critiques of this manuscript.

References

Becker, F. (1987). The impact of spectral emissivity on the measurement of land surface temperature from a satellite. *International Journal of Remote Sensing*, *8*, 1509–1522.

François, C., & Ottlé, C. (1996). Atmospheric corrections in the thermal infrared: global and water vapor dependent split-window algorithms—applications to ASTR and AVHRR data. *IEEE Transactions on Geoscience and Remote Sensing*, *34*, 457–470.

Gallo, K. P., & Tarpley, J. D. (1996). The comparison of vegetation index and surface temperature composites for urban heat-island analysis. *International Journal of Remote Sensing*, *17*, 3071–3076.

Henry, J. A., Dicks, S. E., Wetterqvist, O. F., & Roguski, S. J. (1989). Comparison of satellite, ground-based, and modeling techniques for analyzing the urban heat island. *Photogrammetric Engineering and Remote Sensing*, *55*, 69–76.

Howard, L. (1833). *The climate of London*, vols. I–III. London: Harvey and Dorton.

Karl, T. R., Diaz, H. F., & Kukla, G. (1988). Urbanization: its detection and effect in the United States climate record. *Journal of Climate*, *1*, 1099–1123.

Kawashima, S., Ishida, T., Minomura, M., & Miwa, T. (2000). Relations between surface temperature and air temperature on a local scale during winter nights. *Journal of Applied Meteorology*, *39*, 1570–1579.

Kidwell, K. B. (1998). *NOAA polar orbiter data users guide*. Washington, DC: U.S. Department of Commerce, NOAA, 20233.

Kłysik, K., & Fortuniak, K. (1999). Temporal and spatial characteristics of the urban heat island of Łódź, Poland. *Atmospheric Environment*, *33*, 3885–3895.

Magee, N., Curtis, J., & Wendler, G. (1999). The urban heat island effect at Fairbanks, Alaska. *Theoretical and Applied Climatology*, *64*, 39–47.

Montávez, J. P., Rodríguez, A., & Jiménez, J. I. (2000). A study of the urban heat island of Granada. *International Journal of Climatology*, *20*, 899–911.

Oke, T. R. (1978). *Boundary layer climates*. London, UK: Methuen & Co.

Owen, T. W., Carlson, T. N., & Gillies, R. R. (1998). An assessment of satellite remotely-sensed land cover parameters in quantitatively describing the climatic effect of urbanization. *International Journal of Remote Sensing*, *19*, 1663–1681.

Prata, A. J. (1993). Land surface temperatures derived from the Advanced Very High Resolution Radiometer and the Along-Track Scanning Radiometer 1, theory. *Journal of Geophysical Research*, *98*, 16689–16702.

Price, J. C. (1984). Land surface temperature measurements from the split window channels of the NOAA 7 Advanced Very High Resolution Radiometer. *Journal of Geophysical Research*, *89*, 7231–7237.

Rees, W. G. (1990). *Physical principles of remote sensing*. Cambridge, UK: Cambridge Univ. Press.

Roth, M., Oke, T. R., & Emery, W. J. (1989). Satellite-derived urban heat islands from three coastal cities and the utilization of such data in urban climatology. *International Journal of Remote Sensing*, *10*, 1699–1720.

Steinecke, K. (1999). Urban climatological studies in the Reykjavík subarctic environment, Iceland. *Atmospheric Environment*, *33*, 4157–4162.

Streutker, D. R. (2002). A remote sensing study of the urban heat island of Houston, Texas. *International Journal of Remote Sensing*, *23*, 2595–2608.

U.S. Bureau of Census (1996). *Land area, population, and density for metropolitan areas: 1990*. Washington, DC: Population Distribution Branch, U.S. Bureau of the Census, 20233.

U.S. Bureau of Census (2001). *Census 2000 Summary file 1*. Washington, DC: Population Distribution Branch, U.S. Bureau of the Census, 20233.

Vidal, A. (1991). Atmospheric and emissivity correction of land surface temperature measured from satellite using ground measurements or satellite data. *International Journal of Remote Sensing*, *12*, 2449–2460.

Wang, W.-C., Zeng, Z., & Karl, T. R. (1990). Urban heat islands in China. *Geophysical Research Letters*, *17*, 2377–2380.